Arabian Journal of Chemistry (2023) **16**, 105122

King Saud University

Arabian Journal of Chemistry

www.ksu.edu.sa
www.sciencedirect.com

ORIGINAL ARTICLE

Synthesis of hierarchical porous carbon sphere via crosslinking of tannic acid with Zn^{2+} for efficient adsorption of methylene blue

Wenping Cao [a], Danni Li [b], Sisuo Zhang [b], Jing Ren [b], Xiaoning Liu [b,*], Xinhua Qi [b,*]

[a] *School of Environmental Engineering, Xuzhou Institute of Technology, Xuzhou 221111, China*
[b] *College of Environmental Science and Engineering, Nankai University, No. 38, Tongyan Road, Jinnan District, Tianjin 300350, China*

Received 8 February 2023; accepted 29 June 2023
Available online 4 July 2023

KEYWORDS

Biomass;
Porous materials;
Tannin acid;
Adsorption;
Dye wastewater

Abstract Hierarchical porous carbon spheres (HPCS) were synthetized utilizing tannic acid as biomass source and Zn^{2+} as cross-linking agent. Metal Zn^{2+} prove to be pivotal in the preparation of materials, which can promote the formation of spherical structure and make materials have both micropores and mesopores. The adsorbent has regular spherical shape, specific surface areas of > 1000 m^2/g, the maximum adsorption capacity (q_{max}) of methylene blue is 697 mg/g. It has stable adsorption performance in a broad pH environment (3–11), and the methylene blue removal remains at 91.9% after five cycles. The hierarchical porous structure is beneficial to the immobilization process of methylene blue, and hydrogen bonding, π-π interaction and electrostatic attraction are the main forces for the immobilization of methylene blue. This research offers a promising way for the exploration of biomass-based materials for efficacious dye removal.

1. Introduction

Organic dyes are typical organic pollutants (Jiao et al., 2022; Xiao et al., 2021; Najafi et al., 2022), which pollute the ecological environment mainly through the following ways: i) Most of the dyes are toxic (such as benzidine dyes, some azo dyes, *etc.*) (Yuan et al., 2022; Albadarin et al., 2017; Chen et al., 2021). The dyes discharged in the environment enter the organism transit the food chain and pose a menace to the health of human beings or other organisms (Li et al., 2022; Kaya-Özkiper et al., 2021; Omrani et al., 2022). ii) For the visual pollution of water color, colored water will not only affect the visual senses, but also prevent sunlight from penetrating the water, weaken the photosynthesis of aquatic organisms, and affect the growth of aquatic organisms (El-Sewify et al., 2022; Ismail et al., 2019; He et al., 2021). iii) When the dye is decomposed in the water environment, it will consume a lot of oxygen, resulting in anoxia, odor and corruption of the water body, which is not conducive to the growth of aquatic animals and plants (Zhu et al., 2019; Khatri et al., 2015;

* Corresponding authors.
E-mail addresses: liuxiaoning@nankai.edu.cn (X. Liu), qixinhua@nankai.edu.cn (X. Qi).
Peer review under responsibility of King Saud University.

Production and hosting by Elsevier

https://doi.org/10.1016/j.arabjc.2023.105122
1878-5352

Alizadeh et al., 2022). Therefore, how to efficiently remove organic, dyes in the water environment has been widely concerned by countries all over the world.

Great effort has been put forward to develop effective technologies for removing organic dyes. Adsorption (Georgouvelas et al., 2021; Brar et al., 2020; R et al., 2022; Alipanahpour Dil et al., 2019), advanced oxidation (Cao et al., 2019), photocatalysis (Heitmann et al., 2016; Parvizi et al., 2019; Sajjadnejad and Haghshenas, 2023), biodegradation (Pereira et al., 2014) and other methods have been explored and utilized to dislodge organic dyes from aqueous environment. Adsorption is recognized as an ideal way to remove pollutants such as dyes by reason of its cost-effective, simplicity and wide application range, et al (Liu et al., 2019; Zhou et al., 2022). Biomass is one of the most aplenty renewable carbon sources on the globe, and the carbon materials prepared from biomass have been extensively applied in the range of dye removal (Yang et al., 2019; Sellaoui et al., 2020; Dil et al., 2016). However, traditional biochar has low porosity, irregular pore structure and single function, which cannot meet the increasing demand of water treatment (Liu et al., 2021; Merdas et al., 2022). If the morphology and function of biochar are designed, the biochar adsorbent with regular morphology, high porosity and cycle stability can be synthesized by improving the preparation and modification methods of materials, which can efficiently remove organic dyes from water (Huang et al., 2022; Banisheykholeslami et al., 2021; Bastami et al., 2020; Bagheri et al., 2019; Tayebee et al., 2020).

Plant polyphenols are common biomass resources widely exist in nature, their content in plants is second only to lignin, cellulose and hemicellulose, mainly in plant fruits, stems, roots and leaves (Liu et al., 2023). Tannic acid is a typical plant polyphenol, which has rich hydroxyl groups in its molecular structure and can link with metal ions to form a puissant plant polyphenol-metal network (Guo et al., 2021). Making use of this characteristic of tannic acid, templates and cross-linking agents can be used to guide plant polyphenols and metals to form a regular coordination network, thus the new biochar materials with specific morphology can be synthesized. Among them, the materials with spherical morphology have strong structural stability, short channel, abundant pore, and are more in line with hydraulics to facilitate their rapid movement and diffusion in water (Xi et al., 2022; Zhu et al., 2017).

In this study, a high-performance carbon sphere adsorbent with hierarchical pore structure was synthesized by utilizing tannic acid as biomass source, Zn^{2+} as metal cross-linking agent, formaldehyde and amphiphilic nonionic surfactant as structure directing agent. By using the typical cationic organic dye (methylene blue) as the target contaminants, the adsorption ability of the synthesized hierarchical porous carbon spheres for methylene blue were studied in combination with adsorption experiments and related adsorption models. The stability of the materials under different adsorption conditions and during recycling were evaluated, at same time the main mechanism of methylene blue removal by the adsorbents was clarified. This work can supply a theoretical foundation for the exploration of efficacious materials for removing cationic dyes.

2. Materials and method

2.1. Reagents

Triblock copolymer nonionic surfactant (F127) and tannic acid were provided from Sigma-Aldrich Co., Ltd. Formaldehyde (CH_2O, 37%), ammonium hydroxide (NH_3šH$_2O$, 25%), methylene blue ($C_{16}H_{18}ClN_3S$, 99.5%), zinc nitrate ($Zn(NO_3)_2{\cdot}H_2O$, 99.9%), sodium hydroxide(NaOH, 98%), hydrochloric acid (HCl, 37%) were provided by Shanghai Maclean Reagent Co., Ltd.. Anhydrous ethanol was provided by Shanghai Meryer biochemical technology Co., Ltd. All chemicals in this study were used directly without further purification.

2.2. Preparation of HPCS materials

The materials were prepared by sol–gel method (Wei et al., 2018). Typically, 0.8 g triblock copolymer nonionic surfactant (F127) and 2 mL ammonium hydroxide were put into 216 mL of ethanol–water mixed solution (volume ratio of ethanol: water = 1: 5.75) and stirred for 45 min at 25 °C. Immediately afterwards, 0.8 g TA (tannic acid) and 2.5 mL FA (formaldehyde) were poured sequentially into the mixed liquor and stirring was continued for 24 h. Then different amounts (0.2, 0.4 and 0.8 g) of $Zn(NO_3)_2{\cdot}H_2O$ were put into 10 mL of ultrapure water and poured dropwise to the mixed solution and vibrated for 24 h. After the vibrating was completed, the mixed solution was transferred to the autoclave and heated with water at 100 °C for 24 h. Then the mixture was centrifuged and the solid part was washed 3 times with ultrapure water, stoved under vacuum for 8 h at 60 °C subsequently. Eventually, the solid precursors were calcined at (600, 900) °C for 2 h under N_2 atmosphere at a heating speed of 2 °C/min. The resulted samples were named as HPCS-A-B, where A is the amount of Zn added and B is the calcination temperature. The sample without Zn was used as a control named as tannin–formaldehyde carbon spheres (TFCS).

2.3. Characterization of materials

The pore characteristics of hierarchical carbon spheres were measured by Micrometrice ASAP 2460 (USA) automatic specific surface area analyzer. The microstructure of hierarchical carbon sphere was characterized by a scanning electron microscope from Carl Zeiss (Germany). Functional groups of the samples were tested with a Fourier transform infrared spectrometer (FT-IR, Thermo Scientific Nicolet IZ10, USA) with KBr as matrix. The charging characteristics of materials surface at different pH were determined by Maivern Zetasizer nano-ZS (UK) equipment. The JEM-2010PLUS Transmission Electron Microscope (Japan) was used for probing the internal microstructure of carbon materials. The Ultima IV X-ray diffractometer (Japan) was used to collect X-ray diffraction patterns to determine the crystal structure of the sample.

2.4. Adsorption experiment

To study the adsorption kinetics of HPCS-A-B materials for methylene blue, 10 mg adsorbents were soaked in 10 mL methylene blue solution (pH = 7) with a concentration of 800 mg/L, and then shaken at 25 °C and 180 rpm. A group of experiments were set up at each time point. The mixture was taken out at (5, 15 and 30) min, (1, 2, 4, 6, 8, 12, 18, 24, 36 and 48) h and separated by 0.22 μm polyether sulfone membrane. The concentration of methylene blue was analyzed by ultraviolet–visible spectrophotometer (Shimadzu UV-1780, Japan) at the maximum absorption wavelength of methylene blue (664 nm) (Liu et al., 2022; Sadiq and Saleh, 2023).

Adsorption isotherms of methylene blue onto the HPCS-A-B materials were explored by put 10 mg of the materials into 10 mL of methylene blue solutions (pH = 7) with diverse ini-

tial concentrations (0–1000 mg/L) (He et al., 2021). The above mixed solution was oscillated at 25 °C for 24 h, and then filtered. The concentration of methylene blue in the separated liquid was detected.

10 mg of HPCS-A-B samples were added in 10 mL of dye solution with diverse initial concentrations. 0.1 M HCl and NaOH were used to adjust the pH (3, 5, 7, 9 and 11) of the solution to study the effect of pH, and the initial concentration of dye solution was 1000 mg/L (Sellaoui et al., 2020). Then, the mixed solution was vibrated for 24 h at 25 °C and filtered, the concentration of methylene blue in liquid part was detected.

Recyclability of HPCS-A-B was examined through 5 cycle experiments in which 0.1 g HPCS material was put into a 10 mL methylene blue solution (5 mg/L) and vibrated at 25 °C for 24 h. The used HPCS material was filtered and separated, then soaked in acidic ethanol solution (pH = 2) and oscillated at 25 °C and 200 rpm for 12 h to desorb the adsorbate (Hameed et al., 2007). The desorbed solid material was stored at 60 °C for 12 h, and then subsequent adsorption–desorption cycle experiment was carried out.

3. Results and discussion

3.1. The preparation of HPCS

Fig. 1 shows the SEM of the porous carbon sphere materials (HPCS) with different Zn addition amount. It can be found that Zn is extremely important for the formation of HPCS sphere structure. Without Zn, the morphology of pure tannin–formaldehyde (TFCS) is irregular and mulberry-like. With the increase of Zn content (0 g-0.4 g), HPCS materials tend to be spherical and the degree of regularity increases, which indicates that the increase of Zn^{2+} in a certain range can promote the formation of HPCS spheres (Fig. 1 b-c). It can be inferred that the coordination between Zn^{2+} and tannic acid is the key for the formation of HPCS spherical materials. As the addition of Zn^{2+} continues to increase (0.8 g), some flocculent particles appeared at the edge of the sphere of HPCS-0.8–900 (Fig. 1 d). This is caused by excessive Zn volatilization. During the calcination process, the Zn precursor is gradually decomposed into ZnO. As the calcination temperature further increases, the ZnO produced in the C skeleton is reduced to Zn at about 820 °C and evaporated at about 900 °C (Wang et al., 2019). When the excessive content of Zn in HPCS, the evaporation of Zn in the calcination process leads to the fall down of the C skeleton in the material.

For the sake of explore the impact of different calcination temperature on the structure and chemical composition of HPCS materials, the TEM and element mapping of HPCS-0.4–600 and HPCS-0.4–900 were tested, as shown in Fig. 2. Both HPCS-0.4–600 and HPCS-0.4–900 have regular spherical structure, and the structure has excellent stability during the calcination process. It can be found from SEM and TEM that there are great quantity of loose pores on the surface of HPCS-0.4–900 (Fig. 1c, 2e) compared with HPCS-0.4–600 (Fig. 2a). Moreover, there is obvious Zn in the element mapping diagram of HPCS-0.4–600, the characteristic peak of ZnO is detected in HPCS-0.4–600 material by XRD (Fig. 3). No obvious Zn was detected in HPCS-0.4–900 (Fig. 2h). At the same time, the XRD pattern of HPCS-0.4–900 material only shows the peaks of carbon at $2\theta = 25°$, and no obvious peaks of Zn can be found (Fig. S1). These shows that the Zn in HPCS is

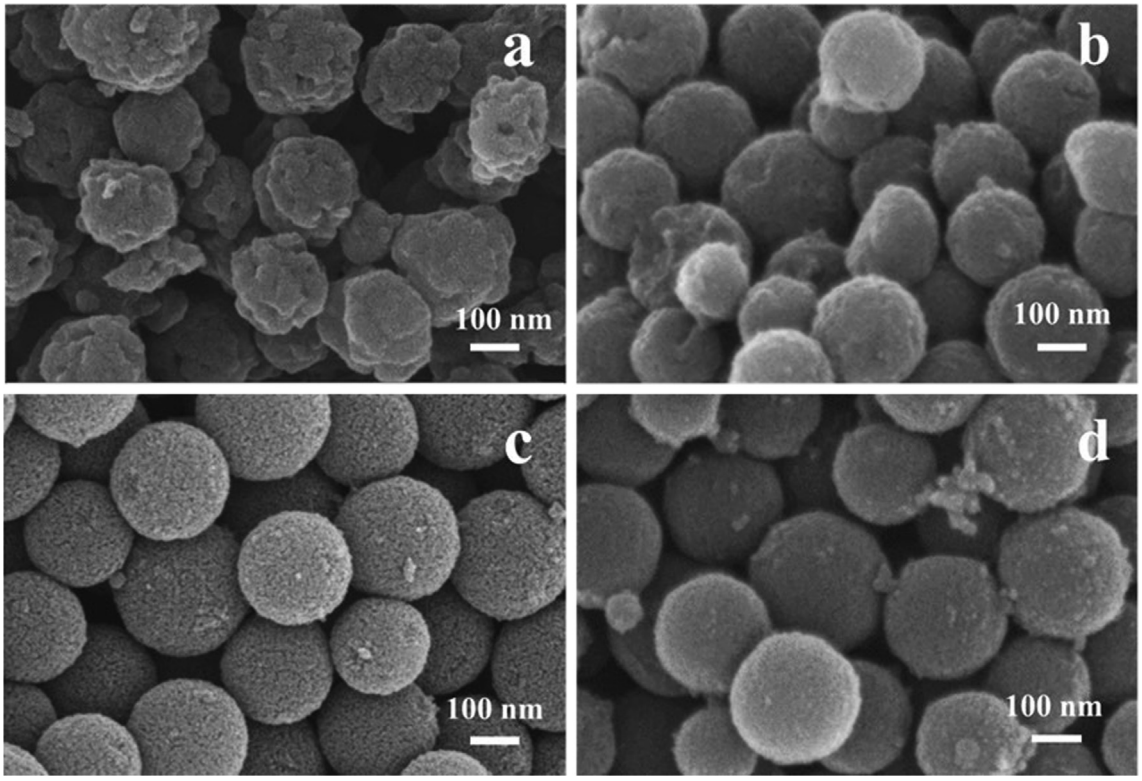

Fig. 1 SEM images of HPCS materials with different Zn additions:(a) TFCS, (b) HPCS-0.2–900, (c) HPCS-0.4–900, (d) HPCS-0.8–900.

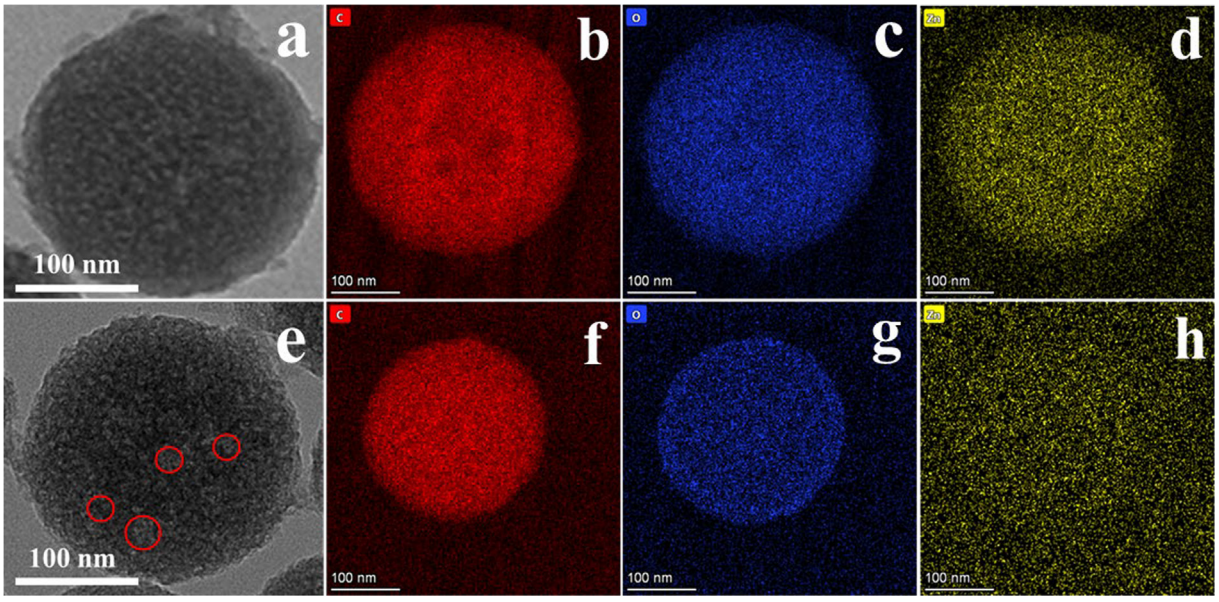

Fig. 2 (a) TEM of HPCS-0.4–600; elemental mappings of HPCS-0.4–600: (b) C, (c) O, (d) Zn; (e) TEM of HPCS-0.4–900; elemental mappings of HPCS-0.4–900: (f) C, (g) O, (h) Zn.

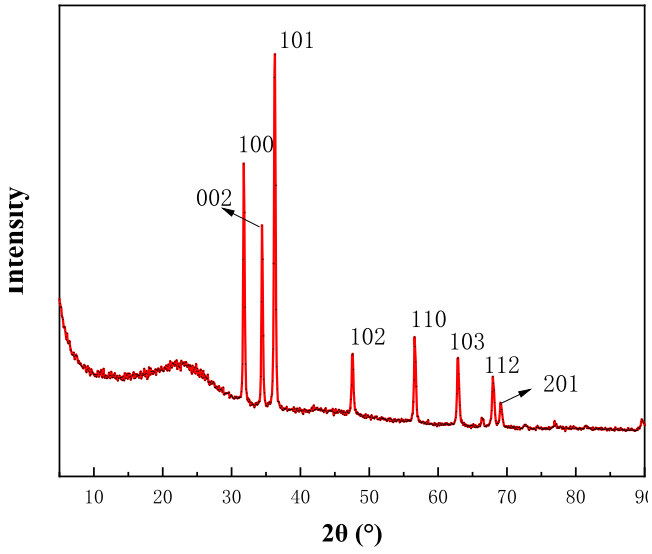

Fig. 3 XRD pattern of HPCS-0.4–600.

evaporated at 900 °C calcination temperature, and this process can produce extensive pores on the surface of the material.

The nitrogen adsorption and desorption isotherms of HPCS materials under different preparation conditions are shown in Fig. 4a. HPCS materials show typical IV isotherms, obvious capillary condensation steps, and H3 hysteresis loop, declaring that the HPCS have the characteristics of crack-like mesoporous structure (Liu et al., 2021; Jiao et al., 2017). The pore size distribution (PSD) of HPCS materials calculated by the BJH model is shown in the Fig. 4b, and the pore structure parameters such as specific surface area (S_{BET}), pore volume, and average pore size are given in Table 1. HPCS materials have a large number of micropores at 0——2 nm besides mesopores at 2.4——7.2 nm, indicating that this kind of materials have hierarchical pore structure, which is be instrumental in adsorption. In the extent of 0.2 to 0.4 g, the increase of Zn significantly broadens the S_{BET} of HPCS materials, and the S_{BET} of HPCS-0.4–900 is 5.24 times that of HPCS-0.2–900. However, when the addition continues to increase (>0.4 g), excessive Zn volatilization leads to the crumble of the C skeleton and the descend of S_{BET} of HPCS materials, which in accordance with that shown in the SEM images (Fig. 1d). In addition, the calcination temperature can also significantly affect the pore characteristics of HPCS. The S_{BET} of HPCS-0.4–600 is 574 m^2/g, while the HPCS-0.4–900 is increased to 1001 m^2/g. Compared with HPCS-0.4–600, the S_{BET} of mesoporous s and micropore in HPCS-0.4–900 increased by 1.17 times and 1.61 times, respectively. This fully shows that the evaporation of Zn is the main reason why HPCS materials have hierarchical pores, and the area of micropores produced is larger than that of mesopores.

The preparation of HPCS is mainly divided into three steps, the process is shown in Fig. 5. i) The-O-in the hydrophilic segment (PEO) of triblock nonionic surfactant (PEO-PPO-PEO, F127) interacts with phenolic hydroxyl groups in tannic acid to form hydrogen bonds (Liu et al., 2022). The continuous addition of formaldehyde can form tannin–formaldehyde-F127 oligomer through phenolic condensation. ii) With the addition of metal ion Zn^{2+}, the oligomers are further condensed to form spherical tannin-Zn polymer through the coordination between phenolic hydroxyl group in tannin molecule and Zn^{2+} (Feng et al., 2022). iii) Hierarchical porous carbon spheres containing ZnO (<820 °C), Zn (820——900 °C) or Zn-free (≥900 °C) are obtained by calcination at different temperatures. The addition of Zn^{2+} and calcination temperature significantly affect the morphology, pore structure and chemical composition of this kind of materials, so the preparation parameters can be adjusted according to the practical application to obtain the materials with the best properties.

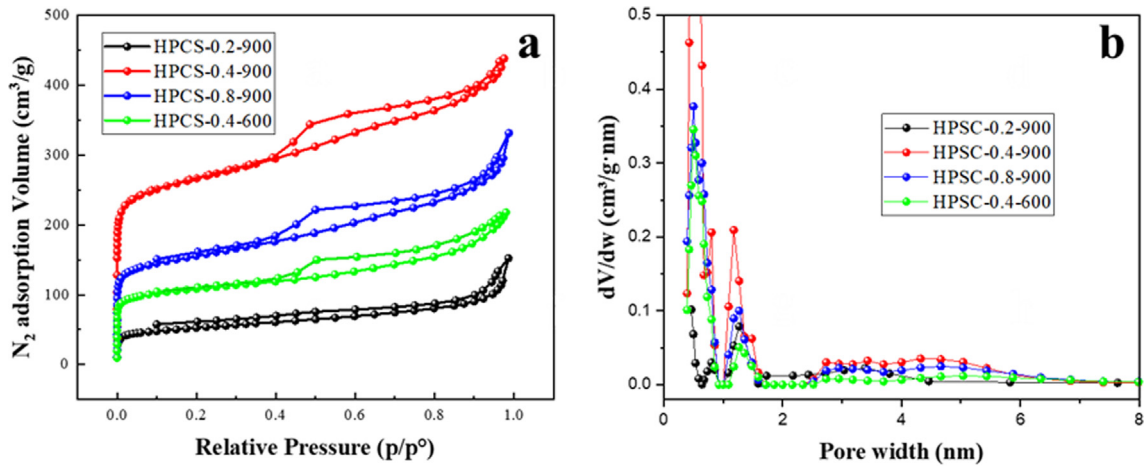

Fig. 4 (a) nitrogen adsorption–desorption curves of HPCS materials; (b) pore size distributions of HPCS materials.

Table 1 Pore size characteristic data of HPCS materials.

Sample	S_{BET} (m^2/g)	Pore volume (cm^3/g)	Average pore size (nm)
HPCS-0.2–900	191	0.243	8.61
HPCS-0.4–900	1001	0.682	4.76
HPCS-0.8–900	574	0.517	3.62
HPCS-0.4–600	405	0.342	3.78

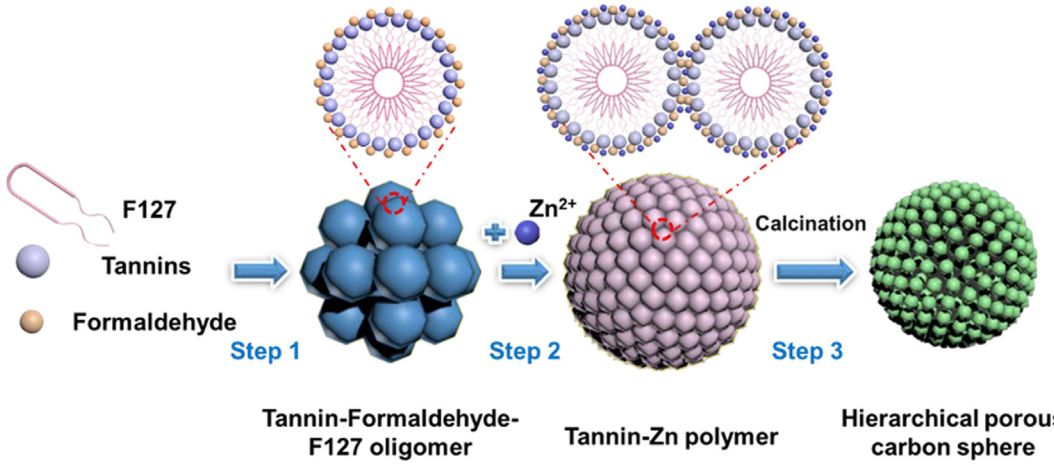

Fig. 5 Schematic diagram of the formation of HPCS materials.

3.2. Adsorption of methylene blue

3.2.1. Adsorption kinetics

The adsorption kinetics of methylene blue on HPCS materials with different preparation parameters was plumbed, and the results are shown in Fig. 6 and Table 2. It can be found that each HPCS material has a fast adsorption rate for methylene blue. The adsorption capacity of HPCS-0.2–900, HPCS-0.4–900, HPCS-0.8–900, and HPCS-0.4–600 to methylene blue solution of 800 mg/L can reach 49.2, 304, 73.3, 51.4 mg/g in 0.5 h, respectively. Furthermore, all HPCS materials can reach adsorption equilibrium after 8 h. HPCS-0.4–900 has the best adsorption performance, which is mainly attributed to its abundant pores, which can tender more space for immobilization of adsorbates. In addition, the removal efficiency of the HPCS material was tested at low dye concentrations (Fig. S2), and it can be found that the material had faster adsorption efficiency at low methylene blue concentrations (10 mg/L), with dye removal efficiency of 100% within 10 min.

The immobilization process of methylene blue can was chopped up into three stages: i) the rapid adsorption stage (0–2 h). In this stage, there are enough adsorption sites in HPCS, methylene blue preferentially and rapidly interact with the active sites on HPCS surface. The adsorption capacity

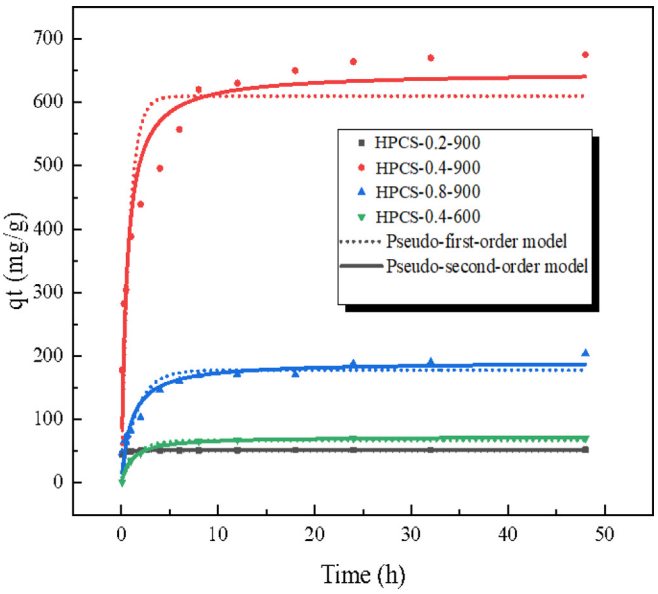

Fig. 6 The adsorption kinetics of methylene blue onto HPCS materials (HPCS dosage: 1 g/L; initial concentration: 800 mg/L; time: 0—48 h; pH = 7; 25 °C).

Table 2 Adsorption kinetic parameters on the HPCS materials.

Adsorbents	Pseudo-first-order model			Pseudo-second-order model		
	k_1	q_e	R^2	k_2	q_e	R^2
HPCS-0.2–900	25	51.3	0.644	0.014	52.7	0.918
HPCS-0.4–900	1.25	610	0.791	0.0028	648	0.910
HPCS-0.8–900	0.63	178	0.835	0.0052	191	0.912
HPCS-0.4–600	0.70	67.5	0.980	0.013	73.1	0.996

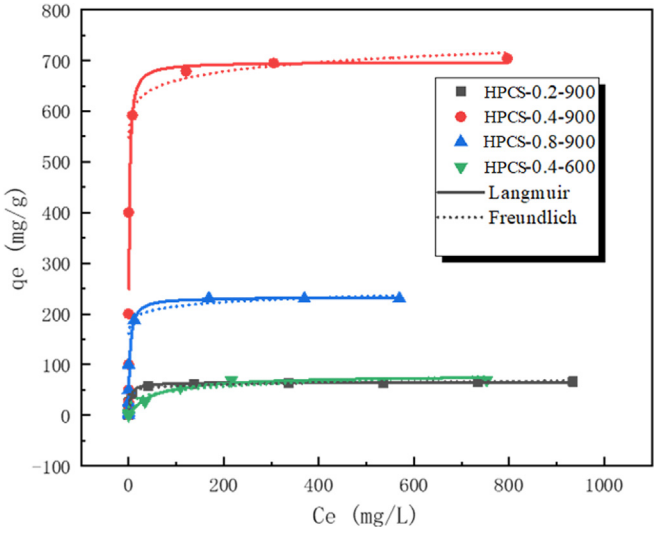

Fig. 7 The adsorption isotherm of HPCS materials. (HPCS dosage: 1 g/L; initial concentration: 0—1000 mg/L; pH = 7; 24 h; 25 °C).

increases linearly with time. ii) Slow adsorption stage (2–8 h), in which the surface active sites of HPCS are occupied in large quantities, and methylene blue molecules need to be combined with the active sites in the internal voids of HPCS through diffusion. At this time, the adsorption rate gradually slows down, the adsorption capacity increases in a curve shape with time.

iii) In the equilibrium adsorption stage (> 8h), the valid site on the surface and interior of HPCS were occupied, and the adsorption and desorption of dye reached equilibrium.

Pseudo-first-order and pseudo-second-order kinetic equations were used to fit the adsorption data to explore the adsorption mechanism of methylene blue on HPCS materials and to evaluate the remove rate of methylene blue on the materials. The specific formulas are as follows:

Pseudo-first-order

$$\ln(q_e\text{-}q_t) = \ln q_e\text{-}k_1 t \quad (1)$$

Pseudo-second-order

$$\frac{t}{q_t} = \frac{1}{k_2 q_e^2} + \frac{1}{q_e} t \quad (2)$$

Where, q_t and q_e are the methylene blue adsorption capacity at t time point and at adsorption equilibrium, respectively, and k_1 and k_2 are the rate constant of the kinetic model, respectively (Liu et al., 2019; Li et al., 2021; Alipanahpour Dil et al., 2019). The kinetic data of methylene blue adsorption on HPCS materials are given in Table 2.

The determination coefficient of pseudo-second-order kinetics ($R^2 \geq 0.910$) of methylene blue adsorption by HPCS is larger than that of pseudo-first-order kinetics ($R^2 \geq 0.644$). The immobilization process is more in accordance with the pseud-second-order kinetic model, which shows that the adsorption of methylene blue by HPCS is mainly chemical adsorption, and there is a sharing or exchange of electrons between the adsorbent and the adsorbate (Liu et al., 2016).

3.2.2. Adsorption isotherm

In order to evaluate the adsorption ability of HPCS to methylene blue and to explore the basic adsorption mechanism, the adsorption properties of HPCS at different initial concentrations of methylene blue were tested (Fig. 7). In addition, the Langmuir and Freundlich isothermal adsorption models were used to fit the adsorption data. The specific equations are as follows:

Langmuir.

$$q_e = K_L q_{max} C_e / (1 + K_L C_e) \quad (3)$$

Freundlich

$$q_e = K_F C_e^n \quad (4)$$

Where, K_L is the characteristic constant of Langmuir adsorption, which indicates the affinity between HPCS materials and methylene blue (Chen et al., 2021); K_F; n are the characteristic constant of Freundlich adsorption, which characterizes the adsorption capacity and adsorption strength, respectively (Zheng et al., 2018); q_e represents the adsorption capacity at adsorption equilibrium; C_e represents the concentration of methylene blue in solution after adsorption equilibrium; q_{max} represents the maximum adsorption capacity of HPCS to methylene blue in the Langmuir isotherm adsorption curve. The data of the isothermal adsorption equation of methylene blue on HPCS materials are given in Table 3.

It can be found that the fitting effect of Langmuir model for methylene blue adsorption of HPCS material ($R^2 \geq 0.947$) is overshoot that of Freundlich equation ($R^2 \geq 0.733$), which indicates that the valid adsorption site of HPCS material is monolayer homogeneous (Shang et al., 2019; Piccin et al., 2012). The maximum adsorption capacity (q_{max}) of HPCS materials acquired from the fitting data of Langmuir model is HPCS-0.4–900 (697 mg/g) > HPCS-0.8–900 (233 mg/g) > HPCS-0.4–600 (79.5 mg/g) > HPCS-0.2–900 (65.2 mg/g). There is a high positive correlation between the q_{max} of HPCS materials and surface area data, which indicates that S_{BET} of the material is the key factor affecting its performance in the process of methylene blue removal. Through the comparison of the removal capacity of HPCS-0.4–900 and other related biochar materials, it is found that the adsorption ability is outstrips that of other materials (Table 4), which further proves that the hierarchical porous carbon spheres have great potential in dye adsorption. Because HPCS-0.4–900 material has the best adsorption ability, it was selected for subsequent adsorption experiments.

3.2.3. The influence of pH

The pH of the water can impact on the surface charge characteristics of materials and the ionization form of pollutant, which is significant factor to interfere with the adsorption performance (Batzias and Sidiras, 2007; Sharifpour et al., 2019). The adsorption performance of HPCS-0.4–900 for methylene blue at different pH is shown in Fig. 8a. With the increase of pH in the reaction system, the adsorption performance of HPCS-0.4–900 showed an upward trend. When the pH of the solution increased from 3 to 11, the methylene blue adsorption capacity of the material increased from 363 to 817 mg/g. This result is mainly produced by the change of surface charge characteristics of HPCS-0.4–900. The charge of HPCS-0.4–900 at different pH is shown in Fig. 8b, from which it can be found that the zero point charge (pHpzc) of HPCS-0.4–900 is 1.6. Methylene blue cationic dyes are positively charged in solution, and when pH < 1.6, the protonation on the surface of the HPCS is also positively charged, which will cause electrostatic repulsion between the material and pollutant, thus affecting the adsorption performance. However, when pH > 1.6, the surface of the material is negatively charged, and with the increase of pH, the negative potential energy of

Table 3 The adsorption isotherm parameters of HPCS materials.

Adsorbents	Langmuir model			Freundlich model		
	K_L	q_{max}	R^2	K_F	n	R^2
HPCS-0.2–900	0.271	65.2	0.979	41	0.073	0.875
HPCS-0.4–900	0.703	697	0.979	553	0.038	0.949
HPCS-0.8–900	0.342	233	0.996	166	0.055	0.899
HPCS-0.4–600	0.019	79.5	0.947	17	0.22	0.733

Table 4 Comparison of the adsorption performance between HPCS and other biomass materials.

Adsorbents	q_{max} (mg/g)	Reference
Cork-based activated carbons	350 (20 °C)	(Novais et al., 2018)
Quebracho tannin gel	483 (20 °C)	(Sánchez-Martín et al., 2010)
Cashew nut shell based carbons	476	(Spagnoli et al., 2017)
Bamboo-based activated carbon	454 (30 °C)	(Hameed et al., 2007)
Carbon nanotubes modified with tannin	202 (25 °C)	(Gan et al., 2018)
Coffee husk based activated carbon	416 (30 °C)	(Tran et al., 2020)
HPCS	697 (25 °C)	This work

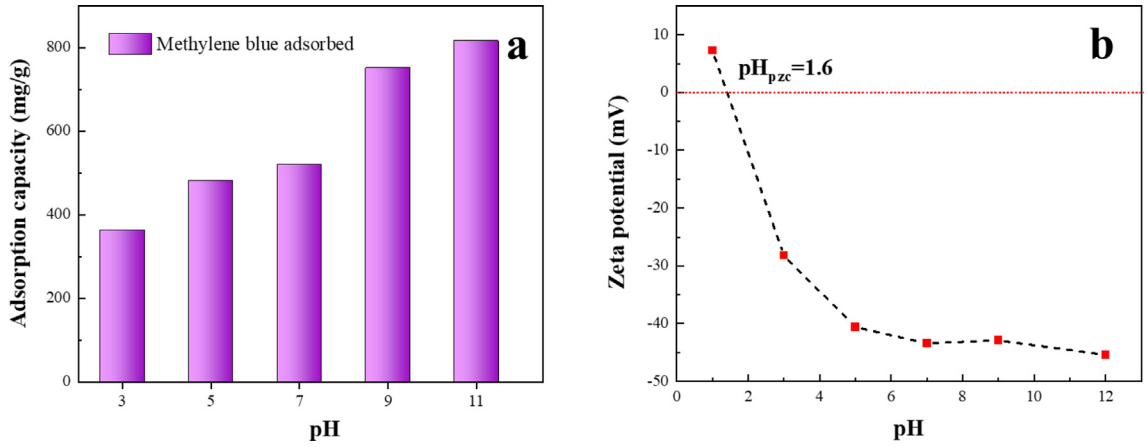

Fig. 8 (a) Effect of pH on the adsorption ability of HPCS material. (HPCS dosage: 1 g/L, initial concentration: 800 mg/L, 24 h, 25 °C), (b) surface charge of the HPCS material at different pH.

the material is crescendo, HPCS-0.4–900 can adsorb more methylene blue by electrostatic action. Generally speaking, HPCS-0.4–900 can maintain high methylene blue adsorption performance (> 363 mg/g) in a broad scope of pH (3–11), so it has broad perspective in practical water treatment applications.

3.2.4. Recycling of HPCS material

In this study, methylene blue was desorbed from HPCS-0.4–900 material by acidic ethanol solution (pH = 2) after adsorption. H^+ in acidic ethanol re-seizes the adsorption site of HPCS-0.4–900 to realize the renewal of material. The reusability and stability of HPCS-0.4–900 material were checked by adsorption–desorption cycle (Fig. 9). After 3 cycles, the methylene blue removal efficiency of HPCS-0.4–900 material was 95.5%. After 5 cycles, the removal efficiency still remained above 91.9%. This shows that HPCS-0.4–900 material can still keep the stability of its adsorption performance after regeneration cycle.

3.3. Adsorption mechanism of methylene blue by HPCS

In an effort to investigate the mechanism of methylene blue adsorption by HPCS, the HPCS samples before and after adsorption were detected by FT-IR, and the results are shown in Fig. 10. After adsorbing methylene blue, the HPCS material shows the stretching vibration peak of C-N in aromatic amine at 1234 cm^{-1}, which belongs to the characteristic peak of methylene blue, indicating that HPCS material can be combined with methylene blue. The stretching vibration peak of –OH in the material has a blue shift before (3435 cm^{-1}) and after adsorption (3437 cm^{-1}), which indicates that hydrogen bonding occurs in the process of adsorption of methylene blue. In addition, methylene blue is an ideal planar molecule, and its aromatic ring is rich in π electrons in its molecular structure, which is generally regarded as an ideal π electron donor (Diagboya et al., 2014; Yang and Cannon, 2022). HPCS material is rich in carbon, and the C = C stretching vibration peak of aromatic ring is detected at 1589 cm^{-1} in FT-IR spectra, so it can be inferred that π-π electron donor–acceptor interaction is another important mechanism of methylene blue adsorption by HPCS. From the kinetic data of methylene blue adsorption by HPCS, it is concluded that the adsorption process is close to the pseudo-second-order kinetic equation, and chemical adsorption is the main mechanism of methylene blue adsorption by HPCS. Hydrogen bonding and π-π interaction should be the main forces for HPCS materials to adsorb methylene blue.

On the other hand, methylene blue is a typical cationic dye (Li et al., 2020; Supelano et al., 2020), which shows positive charge in aqueous solution, while HPCS materials show negative charge in a wide range of pH environments (1.6——14). Electrostatic interaction is another force for the fixation of methylene blue in HPCS materials. It is worth noting that metals usually show positive charge in aqueous solution, and load-

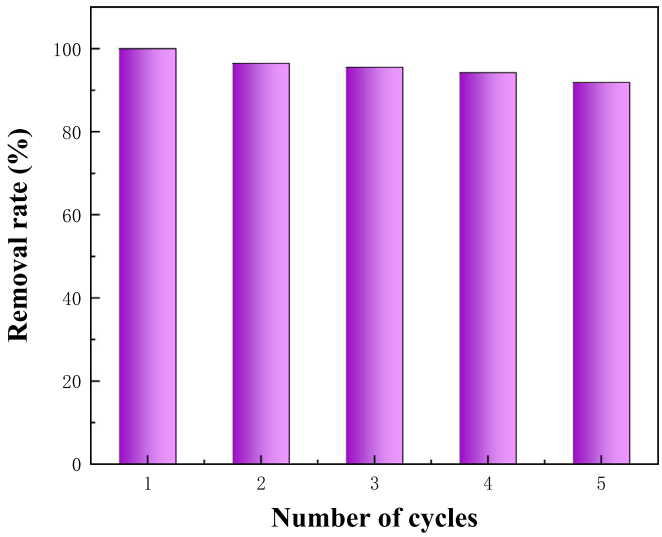

Fig. 9 Adsorption capacity of methylene blue on HPCS material in 5 cycles. (HPCS dosage: 1 g/L, initial concentration: 100 mg/L, 24 h, 25 °C).

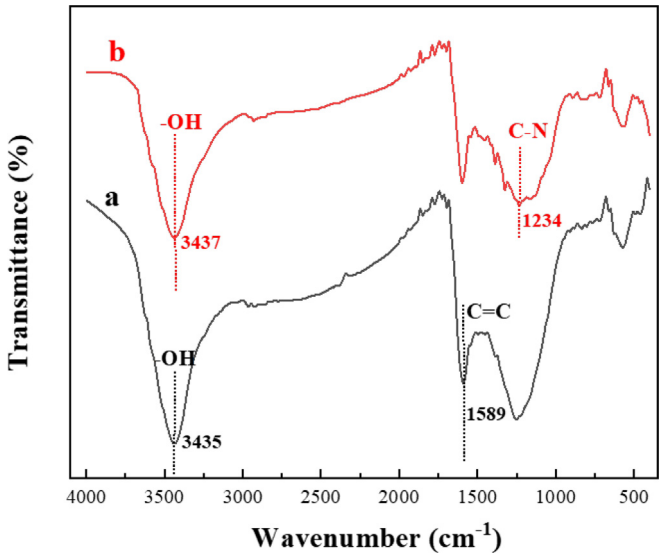

Fig. 10 FT-IR spectra of HPCS before and after adsorption of methylene blue (a) before adsorption; (b) after adsorption.

ing metals in carbon materials will affect the adsorption performance of methylene blue to some extent, which is one reason why the adsorption performance of HPCS-0.4–900 (pure carbon material) is much higher than that of HPCS-0.4–600 (contains ZnO).

It is known that methylene blue has a two-dimensional molecular structure with a molecular size of 1.43 nm × 0.61 n m × 0.40 nm. Flat methylene blue molecules can be inserted into micropores (< 2 nm) (Zhu et al., 2016). Moreover, when the molecular size of the adsorbate is close to the pore size of the adsorbent, the adsorption force can be strengthened by the overlapping adsorption potential of the relative pore wall, that is, the pore filling mechanism (Shi et al., 2022). HPCS material has a hierarchical porous structure, which can capture a large number of methylene blue molecules through diffusion, and its micropores can further hold methylene blue molecules through the pore filling mechanism. Zn is the key to the formation of HPCS hierarchical porous structure, which plays a dual role in the preparation of HPCS materials: i) in the process of material preparation, Zn^{2+} can be used as a cross-linking agent to ensure the formation of spherical morphology of HPCS; ii) during the calcination process (≥900 °C), the evaporation of Zn can produce both micropores and mesopores on the surface of HPCS, and the micropore area is larger than the mesoporous area, which is beneficial to enhance the adsorption of methylene blue on HPCS materials. The overall mechanism of methylene blue adsorption by HPCS is shown in the Fig. 11.

4. Conclusion

In this study, new hierarchical porous carbon spheres (HPCS) were prepared using biomass tannic acid as precursor, metal Zn^{2+} as cross-linking agent. Metal Zn plays a dual role, which can promote

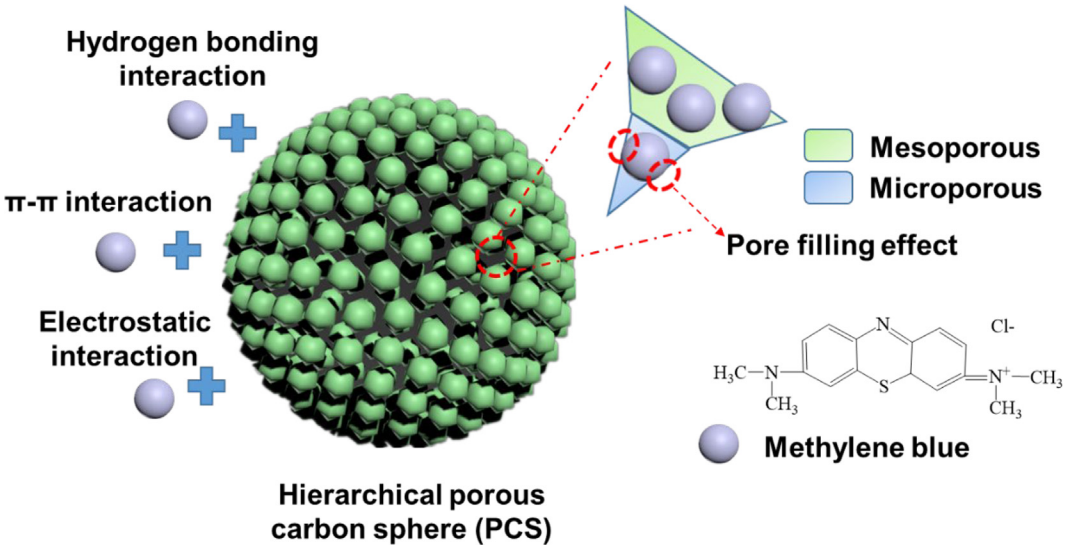

Fig. 11 The overall adsorption mechanism of methylene blue by HPCS material.

the formation of HPCS spherical structure and make the material surface have hierarchical pore structure of both mesoporous and microporous. HPCS material showed excellent performance in the application of methylene blue adsorption that the maximum adsorption capacity was as high as 697 mg/g, and the methylene blue removal rate remained above 91.9% after 5 cycles. The study confirmed that hydrogen bonding, π-π interactions and electrostatic interactions are the main mechanisms of methylene blue adsorption by HPCS materials, and its hierarchical pore structure is favorable to the adsorption process of methylene blue. This work provides a synthesis strategy of hierarchical porous carbon spheres, which has immense application potential in the field of pollutant adsorption. Subsequent research should be strengthened for many types of dye pollutants and in the complex environment of real wastewater.

Declaration of Competing Interest

The authors declare that they have no known competing financial interests or personal relationships that could have appeared to influence the work reported in this paper.

Acknowledgements

The authors gratefully acknowledge financial support of the National Natural Science Foundation of China (42207067 and 22178181), the Natural Science Fund of Tianjin (No. 21JCZDJC00180), the Fundamental Research Funds for the Central Universities (Nankai University (No. 63231085)), Key University Science Research Project of Jiangsu Province (No. 20KJA610004) and Technological Innovation Projects of Xuzhou (KC21282).

Appendix A. Supplementary material

Supplementary data to this article can be found online at https://doi.org/10.1016/j.arabjc.2023.105122.

References

Albadarin, A.B. et al, 2017. Activated lignin-chitosan extruded blends for efficient adsorption of methylene blue. Chem. Eng. J. 307, 264–272.

Alipanahpour Dil, E. et al, 2019. Efficient adsorption of Azure B onto CNTs/Zn:ZnO@Ni2P-NCs from aqueous solution in the presence of ultrasound wave based on multivariate optimization. J. Ind. Eng. Chem. 74, 55–62.

Alipanahpour Dil, E. et al, 2019. Synthesis and application of Ce-doped TiO2 nanoparticles loaded on activated carbon for ultrasound-assisted adsorption of Basic Red 46 dye. Ultrason. Sonochem. 58, 104702.

Alizadeh, K., Khaledyan, E., Mansourpanah, Y., 2022. Novel modified magnetic mesopouros silica for rapid and efficient removal of methylene blue dye from aqueous media. J. Appl. Organomet. Chem. 2 (4), 198–208.

Bagheri, R. et al, 2019. RSM-CCD design of malachite green adsorption onto activated carbon with multimodal pore size distribution prepared from Amygdalus scoparia: Kinetic and isotherm studies. Polyhedron 171, 464–472.

Banisheykholeslami, F., Hosseini, M., Najafpour Darzi, G., 2021. Design of PAMAM grafted chitosan dendrimers biosorbent for removal of anionic dyes: Adsorption isotherms, kinetics and thermodynamics studies. Int. J. Biol. Macromol. 177, 306–316.

Bastami, T.R., Khaknahad, S., Malekshahi, M., 2020. Sonochemical versus reverse-precipitation synthesis of CuxO/Fe2O3/MoC nanohybrid: removal of reactive dyes and evaluation of smartphone for colorimetric detection of organic dyes in water media. Environ. Sci. Pollut. Res. 27 (9), 9364–9381.

Batzias, F.A., Sidiras, D.K., 2007. Simulation of dye adsorption by beech sawdust as affected by pH. J. Hazard. Mater. 141 (3), 668–679.

Brar, S.K., Wangoo, N., Sharma, R.K., 2020. Enhanced and selective adsorption of cationic dyes using novel biocompatible self-assembled peptide fibrils. J. Environ. Manage. 255, 109804.

Cao, Y. et al, 2019. Biowaste-derived bimetallic Ru–MoOx catalyst for the direct hydrogenation of furfural to tetrahydrofurfuryl alcohol. ACS Sustain. Chem. Eng. 7 (15), 12858–12866.

Chen, X. et al, 2021. Chlorophenols in textile dyeing sludge: Pollution characteristics and environmental risk control. J. Hazard. Mater. 416, 125721.
Chen, Y. et al, 2021. Hydroxyapatite modified sludge-based biochar for the adsorption of Cu2+ and Cd2+: Adsorption behavior and mechanisms. Bioresour. Technol. 321, 124413.
Diagboya, P.N. et al, 2014. Graphene oxide–tripolyphosphate hybrid used as a potent sorbent for cationic dyes. Carbon 79, 174–182.
Dil, E.A. et al, 2016. Modeling and optimization of Hg2+ ion biosorption by live yeast Yarrowia lipolytica 70562 from aqueous solutions under artificial neural network-genetic algorithm and response surface methodology: kinetic and equilibrium study. RSC Adv. 6 (59), 54149–54161.
El-Sewify, I.M. et al, 2022. Superior adsorption and removal of aquaculture and bio-staining dye from industrial wastewater using microporous nanocubic Zn-MOFs. Microporous Mesoporous Mater. 329, 111506.
Feng, Y., Li, P., Wei, J., 2022. Engineering functional mesoporous materials from plant polyphenol based coordination polymers. Coord. Chem. Rev. 468, 214649.
Gan, D. et al, 2018. Facile preparation of functionalized carbon nanotubes with tannins through mussel-inspired chemistry and their application in removal of methylene blue. J. Mol. Liq. 271, 246–253.
Georgouvelas, D. et al, 2021. All-cellulose functional membranes for water treatment: Adsorption of metal ions and catalytic decolorization of dyes. Carbohydr. Polym. 264, 118044.
Guo, Y.X. et al, 2021. Polyphenol-containing nanoparticles: synthesis, properties, and therapeutic delivery. Adv. Mater. 33 (22), 2007356.
Hameed, B.H., Din, A.T.M., Ahmad, A.L., 2007. Adsorption of methylene blue onto bamboo-based activated carbon: Kinetics and equilibrium studies. J. Hazard. Mater. 141 (3), 819–825.
He, T. et al, 2021. Adsorption characteristics of methylene blue by a dye-degrading and extracellular polymeric substance -producing strain. J. Environ. Manage. 288, 112446.
Heitmann, A.P. et al, 2016. Nanostructured niobium oxyhydroxide dispersed Poly (3-hydroxybutyrate) (PHB) films: Highly efficient photocatalysts for degradation methylene blue dye. Appl. Catal. B: Environ. 189, 141–150.
Huang, F. et al, 2022. Wheat straw-core hydrogel spheres with polypyrrole nanotubes for the removal of organic dyes. J. Clean. Prod. 344, 131100.
Ismail, M. et al, 2019. Pollution, toxicity and carcinogenicity of organic dyes and their catalytic bio-remediation. Curr. Pharm. Des. 25 (34), 3645–3663.
Jiao, Y. et al, 2017. Synthesis of benzxazine-based nitrogen-doped mesoporous carbon spheres for methyl orange dye adsorption. J. Porous Mater. 24 (6), 1565–1574.
Jiao, W. et al, 2022. Construction of imide-functionalized aromatic conjugation tetracarboxylate frameworks and adsorption behavior for iodine and selective cationic dyes. Microporous Mesoporous Mater. 345, 112273.
Kaya-Özkiper, K., Uzun, A., Soyer-Uzun, S., 2021. Red mud- and metakaolin-based geopolymers for adsorption and photocatalytic degradation of methylene blue: Towards self-cleaning construction materials. J. Clean. Prod. 288, 125120.
Khatri, A. et al, 2015. A review on developments in dyeing cotton fabrics with reactive dyes for reducing effluent pollution. J. Clean. Prod. 87, 50–57.
Li, Y. et al, 2020. Solvent-free synthesis of magnetic biochar and activated carbon through ball-mill extrusion with Fe3O4 nanoparticles for enhancing adsorption of methylene blue. Sci. Total Environ. 722, 137972.
Li, S. et al, 2021. A review on biomass-derived CO2 adsorption capture: Adsorbent, adsorber, adsorption, and advice. Renew. Sustain. Energy Rev. 152, 111708.
Li, L. et al, 2022. Enhance pore structure of cyanobacteria-based porous carbon by polypropylene to improve adsorption capacity of methylene blue. Bioresour. Technol. 343, 126101.
Liu, J. et al, 2016. Immobilization of dye pollutants on iron hydroxide coated substrates: kinetics, efficiency and the adsorption mechanism. J. Mater. Chem. A 4 (34), 13280–13288.
Liu, X. et al, 2019. Black liquor-derived calcium-activated biochar for recovery of phosphate from aqueous solutions. Bioresour. Technol. 294, 122198.
Liu, X. et al, 2021. High-capacity structured MgO-Co adsorbent for removal of phosphorus from aqueous solutions. Chem. Eng. J. 426, 131381.
Liu, X.N. et al, 2021. Mg-coordinated self-assembly of MgO-doped ordered mesoporous carbons for selective recovery of phosphorus from aqueous solutions. Chem. Eng. J. 406, 126748.
Liu, X. et al, 2022. Synthesis of self-renewing Fe(0)-dispersed ordered mesoporous carbon for electrocatalytic reduction of nitrates to nitrogen. Sci. Total Environ. 836, 155640.
Liu, X. et al, 2023. Plant polyphenol-derived ordered mesoporous carbon materials via metal ion cross-linking. Carbon 202, 90–100.
Liu, Z., Azharul Islam, M., Huang, J., 2022. Study of the adsorption of methylene blue by phytoremediation-plant biomass carbon. J. Mol. Liq. 366, 120273.
Liu, X., Shen, F., Qi, X., 2019. Adsorption recovery of phosphate from aqueous solution by CaO-biochar composites prepared from eggshell and rice straw. Sci. Total Environ. 666, 694–702.
Merdas, S.M., W. Al-Graiti, and A.S.A. Al-Ameer, *Using PVA@WNS Composite as Adsorbent for Methylene Blue Dye from Aqueous Solutions*. Journal of Medicinal and Chemical Sciences, 2022. **5**(7 (Special Issue)): 1289-1298.
Najafi, M. et al, 2022. Sono-sorption versus adsorption for the removal of congo red from aqueous solution using NiFeLDH/Au nanocomposite: Kinetics, thermodynamics, isotherm studies, and optimization of process parameters. J. Ind. Eng. Chem. 116, 489–503.
Novais, R.M. et al, 2018. Extremely fast and efficient methylene blue adsorption using eco-friendly cork and paper waste-based activated carbon adsorbents. J. Clean. Prod. 197, 1137–1147.
Omrani, E. et al, 2022. Novel ZnTi LDH/h-BN nanocomposites for removal of two different organic contaminants: Simultaneous visible light photodegradation of Amaranth and Diazepam. J. Water Process Eng. 47, 102581.
Parvizi, E. et al, 2019. Photocatalytic efficacy of supported tetrazine on MgZnO nanoparticles for the heterogeneous photodegradation of methylene blue and ciprofloxacin. RSC Adv. 9 (41), 23818–23831.
Pereira, R.A. et al, 2014. Carbon based materials as novel redox mediators for dye wastewater biodegradation. Appl. Catal. B: Environ. 144, 713–720.
Piccin, J.S. et al, 2012. Kinetics and isotherms of leather dye adsorption by tannery solid waste. Chem. Eng. J. 183, 30–38.
R, S.B. and P. K, A novel adsorption process for the removal of salt and dye from saline textile industrial wastewater using a three-stage reactor with surface modified adsorbents. Journal of Environmental Chemical Engineering, 2022. **10**(6): 108729.
Sadiq, Y.K., Saleh, K.A., 2023. Synthesis and characterization of chrome(VI) ion/iron oxide/chitosan composite for oxidation of methylene blue by photo-fenton reaction. Chem. Methodol. 7 (2), 112–122.
Sajjadnejad, M., Haghshenas, S.M.S., 2023. Metal organic frameworks (MOFs) and their application as photocatalysts: Part II. Characterization and photocatalytic behavior. Adv. J. Chem.-Sect. A 6 (2), 172–187.
Sánchez-Martín, J. et al, 2010. Novel tannin-based adsorbent in removing cationic dye (Methylene Blue) from aqueous solution. Kinetics and equilibrium studies. J. Hazard. Mater. 174 (1), 9–16.
Sellaoui, L. et al, 2020. Insights of the adsorption mechanism of methylene blue on brazilian berries seeds: Experiments, phenomenological modelling and DFT calculations. Chem. Eng. J. 394, 125011.

Shang, Y. et al, 2019. Regenerated WO2.72 nanowires with superb fast and selective adsorption for cationic dye: Kinetics, isotherm, thermodynamics, mechanism. J. Hazard. Mater. 379, 120834.
Sharifpour, E. et al, 2019. Optimizing adsorptive removal of malachite green and methyl orange dyes from simulated wastewater by Mn-doped CuO-Nanoparticles loaded on activated carbon using CCD-RSM: Mechanism, regeneration, isotherm, kinetic, and thermodynamic studies. Appl. Organomet. Chem. 33 (3), e4768.
Shi, J. et al, 2022. High-performance biochar derived from the residue of Chaga mushroom (Inonotus obliquus) for pollutants removal. Bioresour. Technol. 344, 126268.
Spagnoli, A.A., Giannakoudakis, D.A., Bashkova, S., 2017. Adsorption of methylene blue on cashew nut shell based carbons activated with zinc chloride: The role of surface and structural parameters. J. Mol. Liq. 229, 465–471.
Supelano, G.I. et al, 2020. Synthesis of magnetic zeolites from recycled fly ash for adsorption of methylene blue. Fuel 263, 116800.
Tayebee, R. et al, 2020. Photodegradation of methylene blue and some emerging pharmaceutical micropollutants with an aqueous suspension of WZnO-NH2@H3PW12O40 nanocomposite. J. Mol. Liq. 317, 113928.
Tran, T.H. et al, 2020. Adsorption isotherms and kinetic modeling of methylene blue dye onto a carbonaceous hydrochar adsorbent derived from coffee husk waste. Sci. Total Environ. 725, 138325.
Wang, G. et al, 2019. Nanoporous carbon spheres derived from metal-phenolic coordination polymers for supercapacitor and biosensor. J. Colloid Interface Sci. 544, 241–248.
Wei, J. et al, 2018. Sol-gel synthesis of metal-phenolic coordination spheres and their derived carbon composites. Angew. Chem.-Int. Ed. 57 (31), 9838–9843.
Xi, R. et al, 2022. Selective hydrogenation of glucose to sorbitol with tannic acid-based porous carbon sphere supported Ni–Ru bimetallic catalysts. Green Energy Environ.
Xiao, W. et al, 2021. Adsorption of organic dyes from wastewater by metal-doped porous carbon materials. J. Clean. Prod. 284, 124773.
Yang, S.-S. et al, 2019. Generation of high-efficient biochar for dye adsorption using frass of yellow mealworms (larvae of Tenebrio molitor Linnaeus) fed with wheat straw for insect biomass production. J. Clean. Prod. 227, 33–47.
Yang, Y., Cannon, F.S., 2022. Biomass activated carbon derived from pine sawdust with steam bursting pretreatment; perfluorooctanoic acid and methylene blue adsorption. Bioresour. Technol. 344, 126161.
Yuan, K. et al, 2022. Facile synthesis and study of functional porous organic polyaminals with ultrahigh adsorption capacities and fast removal rate for rhodamine B dye. Microporous Mesoporous Mater. 344, 112234.
Zheng, J.-J. et al, 2018. Theoretical insight into gate-opening adsorption mechanism and sigmoidal adsorption isotherm into porous coordination polymer. J. Am. Chem. Soc. 140 (42), 13958–13969.
Zhou, Y. et al, 2022. In situ formation of tannic (TA)-aminopropyltriethoxysilane (APTES) nanospheres on inner and outer surface of polypropylene membrane toward enhanced dye removal capacity. Chem. Eng. J. 433, 133843.
Zhu, J. et al, 2016. Nitrogen-enriched, ordered mesoporous carbons for potential electrochemical energy storage. J. Mater. Chem. A 4 (6), 2286–2292.
Zhu, Y. et al, 2017. Fast and high-capacity adsorption of Rb + and Cs + onto recyclable magnetic porous spheres. Chem. Eng. J. 327, 982–991.
Zhu, J. et al, 2019. Adsorption of phosphate and photodegradation of cationic dyes with BiOI in phosphate-cationic dye binary system. Sep. Purif. Technol. 223, 196–202.